

# Mitochondria-Targeting Oxidovanadium(IV) Complex as a Near-IR Light Photocytotoxic Agent

Puja Prasad,<sup>[a]</sup> Imran Khan,<sup>[b]</sup> Paturu Kondaiah,<sup>\*,[b]</sup> and Akhil R. Chakravarty<sup>\*,[a]</sup>

**Abstract:** Oxidovanadium(IV) complexes [VO(L<sup>1</sup>)(phen)]·Cl (**1**) and [VO(L<sup>2</sup>)(L<sup>3</sup>)]·Cl (**2**), in which HL<sup>1</sup> is 2-[(benzimidazol-2-yl)methylimino]-methylphenol (sal-ambmz), HL<sup>2</sup> is 2-[(1-[(anthracen-9-yl)methyl]-benzimidazol-2-yl)methylimino]-methylphenol (sal-an-ambmz), phen is 1,10-phenanthroline and L<sup>3</sup> is dipyrido[3,2-a:2',3'-c]phenazine (dppz) conjugated to a Gly-Gly-OMe dipeptide moiety, were prepared, characterized, and their DNA binding, photoinduced DNA-cleavage, and photocytotoxic properties were studied. Fluorescence microscopy studies were performed by using complex **2** in HeLa and HaCaT cells. Com-

plex **1**, structurally characterized by X-ray crystallography, has a vanadyl group in VO<sub>2</sub>N<sub>4</sub> core with the VO<sup>2+</sup> moiety bonded to N,N-donor phen and a N,N,O-donor Schiff base. Complex **2**, having an anthracenyl fluorophore, showed fluorescence emission bands at 397, 419, and 443 nm. The complexes are redox-active exhibiting the V(IV)/V(III) redox couple near -0.85 V versus SCE in DMF 0.1 M tetrabutylammonium perchlorate (TBAP). Com-

plex **2**, having a dipeptide moiety, showed specific binding towards poly-(dAdT)<sub>2</sub> sequence. The dppz-Gly-Gly-OMe complex showed significant DNA photocleavage activity in red light of 705 nm through a hydroxyl radical (·OH) pathway. Complex **2** showed photocytotoxicity in HaCaT and HeLa cells in visible light (400–700 nm) and red light (620–700 nm), however, the complex was less toxic in the dark. Fluorescence microscopy revealed the localization of complex **2** primarily in mitochondria. Apoptosis was found to occur inside mitochondria (intrinsic pathway) caused by ROS generation.

**Keywords:** apoptosis · bioinorganic chemistry · cell imaging · DNA · photodynamic therapy

## Introduction

Photodynamic therapy (PDT) has emerged as a prospective alternative to chemotherapy by selectively killing tumor cells, leaving the unexposed healthy cells minimally affected.<sup>[1–7]</sup> Photofrin is the FDA-approved PDT drug for treating cancer.<sup>[1,2]</sup> The macrocyclic porphyrin dyes suffer from various side effects such as prolonged skin sensitivity and hepatotoxicity.<sup>[8]</sup> This has necessitated the design of new metal-based PDT agents fulfilling some major requirements of PDT, such as the use of near-IR light in photoactivation. The porphyrin derivatives follow type II pathway requiring high quantum yield ( $\phi$ ) of <sup>1</sup>O<sub>2</sub> production through energy transfer.<sup>[9]</sup> In contrast, redox-active metal complexes could provide an alternative reaction pathway by forming hydrox-

yl radical (·OH) as the reactive oxygen species (ROS) in a photo-redox pathway or by photo-generating other reactive species.<sup>[10–14]</sup>

An important criterion for a PDT drug to be therapeutically effective is to have photoactivation in the near-IR red light for maximum tissue penetration. Also, a desirable oncological aspect in PDT is to have significant localization of the photosensitizer in the cell organelles other than in the nucleus. Localization of the drug in cytoplasmic organelles is preferred because it reduces the possibility of mutation and avoids any potential damage to nuclear DNA. To achieve this, a promising target for anticancer therapy is the mitochondria due to its role in the intrinsic pathway of cell death by apoptosis.<sup>[15–17]</sup> The PDT drug photofrin is known to accumulate in the mitochondrial region.<sup>[18]</sup>

Cancer cells with a high proliferation rate are known to evade apoptosis and, therefore, targeting either the extrinsic or intrinsic pathway to induce apoptosis in cancer cells by a strategically designed PDT agent would be a new way to regress the tumour. This targeting is likely to depend on the sub-cellular localization of the photosensitizers in the cells.<sup>[19]</sup> Because the intrinsic pathway of apoptosis largely depends on the mitochondria, by targeting mitochondria with a suitably designed compound could lead to desirable photoinduced cytotoxicity.<sup>[20]</sup> Besides, mitochondria-targeting anticancer agents are likely to overcome the resistance mechanism that are involved in the conventional chemotherapeutic drug action and would increase the potential of the

[a] P. Prasad, A. R. Chakravarty  
Department of Inorganic and Physical Chemistry  
Indian Institute of Science, Bangalore 560012, Karnataka (India)  
Fax: (+91) 80-23600683  
E-mail: arc@ipc.iisc.ernet.in

[b] I. Khan, Prof. P. Kondaiah  
Department of Molecular Reproduction  
Development and Genetics, Indian Institute of Science  
Bangalore-560012, Karnataka (India)  
Fax: (+91) 80-23600999,  
E-mail: paturu@mrdg.iisc.ernet.in

Supporting information for this article is available on the WWW under <http://dx.doi.org/10.1002/chem.201303487>.

drug. We have been successful in designing and synthesizing an oxidovanadium(IV) complex that shows an unprecedented dual effect of specifically targeting the mitochondria and near-IR light-induced photocytotoxicity in HaCaT and HeLa cancer cells with low dark toxicity.

## Results and Discussion

**Synthesis and general aspects:** Oxidovanadium(IV) complexes  $[\text{VO}(\text{L}^1)(\text{phen})]\cdot\text{Cl}$  (**1**) and  $[\text{VO}(\text{L}^2)(\text{L}^3)]\cdot\text{Cl}$  (**2**), in which  $\text{HL}^1$  is 2-[[[(benzimidazol-2-yl)methylimino]-methyl]-phenol (sal-ambmz),  $\text{HL}^2$  is 2-[[[(1-[(anthracen-9-yl)methyl]-benzimidazol-2-yl)methylimino]-methyl]phenol (sal-an-ambmz), phen is 1,10-phenanthroline, and  $\text{L}^3$  is dipyrro[3,2-a:2',3'-c]phenazine (dppz) conjugated to a dipeptide Gly-Gly-OMe moiety, were prepared in about 70% yield from a general reaction in which the Schiff-base ligand is treated with vanadyl chloride in methanol followed by addition of the heterocyclic base (Figure 1). Two new ligands were pre-

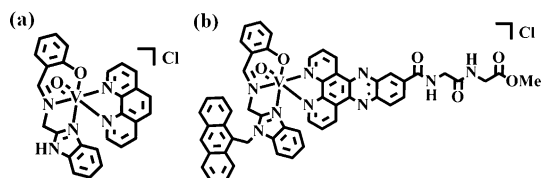


Figure 1. A schematic drawing of complex **1** (a) and complex **2** (b).

pared and characterized (Scheme S1 and Figure S1–S7, the Supporting Information). The ESI-MS of **1** and **2** in MeOH showed essentially a single mass peak at  $m/z = 497.33$  and  $961.53$ , respectively (Figures S8 and S9, the Supporting Information). The  $3d^1$ -oxidovanadium(IV) complexes are one-electron paramagnetic with a magnetic moment value of  $\approx 1.6 \mu_B$  in the solid state at  $25^\circ\text{C}$ . The complexes showed characteristic vanadyl ( $\text{V}=\text{O}$ ) band at  $\approx 964 \text{ cm}^{-1}$ , a  $\text{C}=\text{N}$  band at  $\approx 1615 \text{ cm}^{-1}$ , and the amide carbonyl group of **2** at  $1655 \text{ cm}^{-1}$  (Figures S10 and S11, the Supporting Information).<sup>[21]</sup> Absorption spectra of the complexes in DMF exhibited a d–d band at  $\approx 680 \text{ nm}$  (Figure 2). Complex  $[\text{VO}(\text{sal-ambmz})(\text{phen})]\cdot\text{Cl}$  (**1**) showed a broad band at  $\approx 400 \text{ nm}$  that corresponds to the LMCT (ligand-to-metal charge transfer) from the phenolate oxygen to an empty d-orbital of vanadium.<sup>[22]</sup> This band gets masked in complex **2** due to intraligand electron-transfer. Complex **2**, having an anthracene appended tridentate ligand, showed intense absorption bands at  $\approx 350$ ,  $370$ , and  $390 \text{ nm}$  (Figure 2).<sup>[23]</sup> It displayed emission bands of the anthracenyl fluorophore at  $397$ ,  $419$ , and  $443 \text{ nm}$  with a fluorescence quantum yield value of  $0.011$  (Table 1, Figure 2). The complexes are 1:1 electrolytic

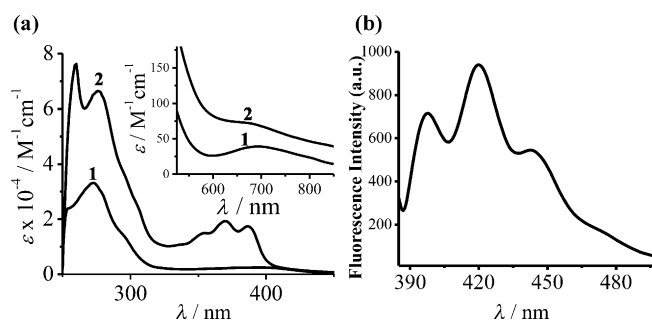


Figure 2. a) UV/Visible spectra of  $[\text{VO}(\text{L}^1)(\text{phen})]\cdot\text{Cl}$  (**1**) and  $[\text{VO}(\text{L}^2)(\text{L}^3)]\cdot\text{Cl}$  (**2**) in DMF with inset showing their d–d bands. b) Fluorescence spectrum of **2** in 2% aqueous DMF ( $\lambda_{\text{exc}}$ ,  $370 \text{ nm}$ ).

in DMF giving a  $\Lambda_M$  value of  $70 \text{ Sm}^2 \text{ M}^{-1}$ . Cyclic voltammograms of the complexes displayed an irreversible V(IV)/V(III) redox process near  $-0.85 \text{ V}$  (vs. SCE) in DMF-0.1 M tetrabutylammonium perchlorate (TBAP) and a quasi-reversible ligand-based redox process at  $-1.06$  and  $-1.56 \text{ V}$  due to dppz-Gly-Gly-OMe (Figure S12, the Supporting Information). Lifetime measurements of the excited state of **2** gave a value of  $9.0 \times 10^{-9} \text{ s}$  (Figure S13, the Supporting Information).

**Crystal structure:** Complex **1** as its  $\text{ClO}_4$  salt (**1a**) was structurally characterized by single-crystal X-ray diffraction technique. Complex **1a**·EtOH crystallized in the  $P\bar{1}$  space group in the triclinic crystal system with two molecules in the unit cell (Figure S14, the Supporting Information). An ORTEP view of the cationic complex is shown in Figure 3.<sup>[24]</sup> The complex with a  $\text{VO}_2\text{N}_4$  core has the  $\text{VO}^{2+}$  moiety bonded to the N,N-donor phen and an N,N,O-donor Schiff base. The V(1)–O(1) distance is  $1.586(4) \text{ \AA}$ . The V(1)–N(2) bond of  $2.326(5) \text{ \AA}$  being *trans* to the  $\text{V}=\text{O}$  group is significantly longer than the other V–N bonds ( $2.130(4)$ – $2.072(5) \text{ \AA}$ , Table S1, the Supporting Information).<sup>[25]</sup> The V–O distance involving the Schiff base is  $1.930(4) \text{ \AA}$ . The Schiff base shows meridional binding mode and phen binds at the axial–equatorial positions of the  $\text{VO}^{2+}$  moiety. The molecular structure of the complex shows that the aromatic rings of phen are not sterically hindered by the ancillary ligand and the phenanthroline base in the complex could efficiently bind to DNA.

**Computational studies:** DFT calculations were performed for complex **2** to obtain the energy-optimized structure and

Table 1. Selected physicochemical data for the complexes **1** and **2**.

Complex	IR <sup>[a]</sup> [ $\text{cm}^{-1}$ ]		Visible <sup>[b]</sup> $\lambda_{\text{max}}$ [nm] ( $\epsilon$ [ $\text{dm}^3 \text{ M}^{-1} \text{ cm}^{-1}$ ])	Emission <sup>[c]</sup> $\lambda_{\text{em}}$	$\Phi_F$ <sup>[d]</sup>	$\Lambda_M$ <sup>[e]</sup> [ $\text{Sm}^2 \text{ M}^{-1}$ ]	$E_i$ [V] <sup>[f]</sup>
	$\nu(\text{C}=\text{N})$	$\nu(\text{V}=\text{O})$					
$[\text{VO}(\text{L}^1)(\text{phen})]\cdot\text{Cl}$ ( <b>1</b> )	1613	960	693(40)	–	–	70	–0.89
$[\text{VO}(\text{L}^2)(\text{L}^3)]\cdot\text{Cl}$ ( <b>2</b> ) <sup>[g]</sup>	1614	964	672 (90)	397, 419, 443	0.011	73	–0.85

[a] In KBr phase. [b] Visible spectral band in DMF. [c] Emission spectra in 2% aq. DMF using  $\lambda_{\text{exc}}$  of  $370 \text{ nm}$ . [d] Fluorescence quantum yield ( $\Phi_F$ ) in 2% aq. DMF. [e]  $\Lambda_M$  = Molar conductance in DMF at  $25^\circ\text{C}$ . [f] Cyclic voltammetric data in DMF using TBAP as a supporting electrolyte at  $50 \text{ mV s}^{-1}$  scan rate. [g] The lifetime of the excited state is  $9.06 \times 10^{-9} \text{ s}$ .

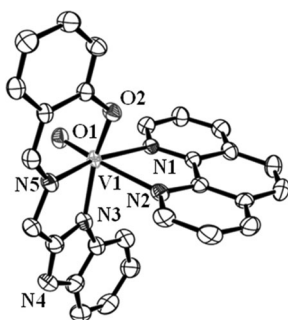


Figure 3. An ORTEP view of the cationic species in  $[\text{VO}(\text{sal-aebmz})\text{-(phen)}][\text{ClO}_4] \cdot 0.5\text{EtOH}$  ( $\mathbf{1} \cdot 0.5\text{EtOH}$ ) showing atom labeling for the metal and hetero-atoms and 50% probability thermal ellipsoids. The hydrogen atoms are not shown for clarity.

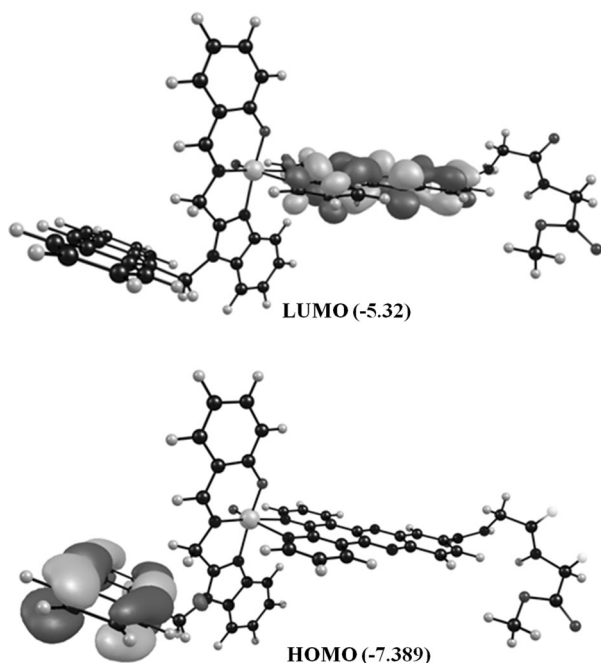


Figure 4. HOMO and LUMO of complex  $\mathbf{2}$  (energy in eV).

to gain insights about its photophysical properties. The energy-optimized views are shown in Figure 4 (see Figure S15, the Supporting Information, for the color figure). The highest occupied molecular orbital (HOMO) and lowest occupied molecular orbital (LUMO), and their energy gap were calculated. The HOMO of  $\mathbf{2}$  lies on the anthracene moiety appended to the tridentate ligand, whereas the LUMO is located on the dppz-Gly-Gly moiety. The LUMO on dppz moiety suggests the involvement of the VO-dppz unit in the photoactivation process. Selected bond distances and angles for the energy-minimized structure of complex  $\mathbf{2}$  from the DFT study are given in Table S2 (the Supporting Information).

**DNA binding:** DNA melting experiments were carried out to study the DNA-binding strengths of the complexes  $\mathbf{1}$  and

$\mathbf{2}$ . The complexes stabilizing the DNA structure result in an increase in the melting temperature. The  $\Delta T_m$  value thus gives an idea about the interaction of the complex with DNA.<sup>[26]</sup> A significant stabilization of calf thymus (ct)-DNA was observed on treatment with complex  $\mathbf{2}$  having a dppz moiety compared with its phen analogue  $\mathbf{1}$  (Figure 5a). The  $\Delta T_m$  values of the complexes are compared to the classical DNA intercalator ethidium bromide (EB) in Table 2. To fur-

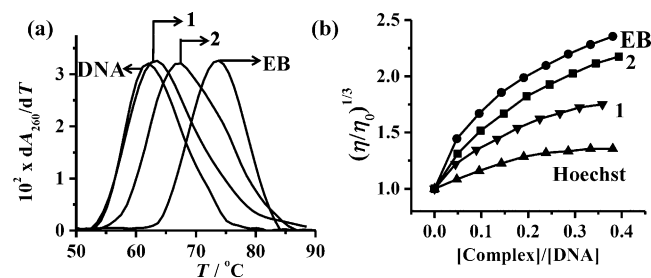


Figure 5. a) Thermal denaturation plots of  $170 \mu\text{M}$  ct-DNA alone and in the presence of the complexes  $\mathbf{1}$  and  $\mathbf{2}$  ( $10 \mu\text{M}$ ) in  $5 \text{ mM}$  Tris-HCl buffer (pH 7.2). b) Effect of increasing the concentration of EB ( $\bullet$ ), complex  $\mathbf{1}$  ( $\blacktriangledown$ ), complex  $\mathbf{2}$  ( $\blacksquare$ ), and Hoechst dye ( $\blacktriangle$ ) on the relative viscosity of ct-DNA ( $140 \mu\text{M}$ ) at  $(37.0 \pm 0.1)^\circ\text{C}$  in Tris-HCl buffer ( $5 \text{ mM}$ , pH 7.2).

Table 2. DNA binding data for the complexes  $\mathbf{1}$  and  $\mathbf{2}$

Complex	$K_b$ [ $\text{M}^{-1}$ ] ct-DNA	$K_b$ [ $\text{M}^{-1}$ ] Poly(dAdT) <sub>2</sub>	$K_b$ [ $\text{M}^{-1}$ ] Poly(dGdC) <sub>2</sub>	$\Delta T_m$ [a] [ $^\circ\text{C}$ ]
$\mathbf{1}$	$3.3 (\pm 0.2) \times 10^4$	–	–	1.5
$\mathbf{2}$	$2.3 (\pm 0.5) \times 10^5$	$1.3 (\pm 0.3) \times 10^6$	$8.3 (\pm 0.4) \times 10^4$	5.1

[a] The value for EB is  $10.8^\circ\text{C}$

ther elucidate the DNA binding nature of the complexes, viscometric titrations were carried out to see the change in the relative viscosity of ct-DNA in presence of the complexes, EB as DNA intercalator and Hoechst 33258 as DNA groove-binder.<sup>[27]</sup> Intercalators result in an elongation of the DNA contour length thus increasing the relative viscosity, whereas minor-groove binder has little effect on the contour length. The plot shown in Figure 5b indicates partial intercalative nature of complex  $\mathbf{2}$ . The intrinsic equilibrium DNA-binding constant ( $K_b$ ) values for complexes  $\mathbf{1}$  and  $\mathbf{2}$  are  $3.3 \times 10^4$  and  $2.3 \times 10^5 \text{ M}^{-1}$ .<sup>[28,29]</sup> The dppz-Gly-Gly-OMe complex  $\mathbf{2}$  showed significantly higher DNA binding strength due to presence of an extended aromatic moiety than its phen analogue. Further, the specificity of  $\mathbf{2}$  towards poly(dAdT)<sub>2</sub> and poly(dGdC)<sub>2</sub> was tested and complex  $\mathbf{2}$  showed higher specificity towards poly(dAdT)<sub>2</sub> binding giving a  $K_b$  value of  $\approx 10^6 \text{ M}^{-1}$  (Table 2 and the Supporting Information, Figure S16).

**DNA cleavage:** The activity of the complexes in photo-damaging DNA was studied using  $50 \mu\text{M}$  of  $\mathbf{1}$  and  $\mathbf{2}$  and supercoiled (SC) pUC19 DNA in Tris-HCl/NaCl buffer containing 10% DMF on photoirradiation with red light of 705 nm wavelength (diode laser).

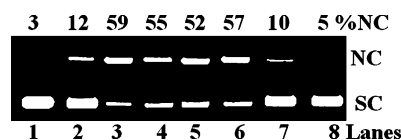


Figure 6. Cleavage of SC pUC19 DNA (0.2  $\mu\text{g}$ , 30  $\mu\text{M}$ ) by complex **2** (50  $\mu\text{M}$ ) in 50 mM Tris-HCl/NaCl buffer (pH 7.2) containing 10% DMF and near-IR light of  $\lambda \approx 705$  nm (40 mW diode laser power) with an exposure time of 2 h: lane 1, DNA control; lane 2, DNA + **1**; lane 3, DNA + **2**; lane 4, DNA + **2** +  $\text{D}_2\text{O}$ ; lane 5, DNA + **2** +  $\text{NaN}_3$ ; lane 6, DNA + **2** + DABCO; lane 7, DNA + **2** + DMSO; lane 8, DNA + **2** + KI.

Complex **2** showed the formation of  $\approx 55\%$  of nicked circular (NC) DNA upon photoirradiation for 2 h (Figure 6). Complex **1** was found to be inactive showing only  $\approx 10\%$  NC DNA formation. Control experiments using the ligands did not show any significant photocleavage of plasmid DNA.

The mechanistic aspects of the DNA photocleavage reactions were investigated by using complex **2** in red light of 705 nm in the presence of various additives, that is, sodium azide and 1,4-diazobicyclo[2.2.2]octane (DABCO) as singlet-oxygen quenchers and DMSO and KI as hydroxyl-radical scavengers (Figure 6). The complex showed photocleavage of DNA only under aerobic medium suggesting the necessity of molecular oxygen and formation of reactive oxygen species (ROS) for its activity. Hydroxyl radical scavengers showed significant reduction in the DNA cleavage activity, whereas no inhibitory effect was observed with singlet-oxygen quenchers. The data suggest formation of hydroxyl radicals, which is also evidenced from the EPR data, showing characteristic four line spectra of a 5,5-dimethyl-1-pyrroline *N*-oxide (DMPO)-OH adduct upon photoirradiation of the complex with red light (Figure S17, the Supporting Information).<sup>[30]</sup>

**Cellular uptake:** Fluorescence-activated cell-sorting (FACS) was performed to monitor the cellular uptake of the fluorescent complex **2** inside human cervical carcinoma (HeLa) and human skin keratinocyte (HaCaT) cell lines.<sup>[31]</sup> A solution of complex **2** (16  $\mu\text{M}$ ) was added to the cells at the interval of 2 and 4 h. The uptake of **2** was found to be more in HaCaT than in HeLa cells (Figure 7a and the Supporting Information, Figure S18). Complex **2** showed  $\approx 90\%$  uptake within 4 h in the cells. FACS data suggest 4 h incubation time suitable for cytotoxicity studies before exposing the samples to light. To standardize the incubation time of the complexes with the cells corresponding to the lowest  $\text{IC}_{50}$  value, we carried out the experiments using HaCaT cells and complex **2** at different incubation times of 1, 2, 4, 6, and 8 h (Figure 7b). We obtained the lowest  $\text{IC}_{50}$  value of 9.4  $\mu\text{M}$  at 4 h incubation time. The  $\text{IC}_{50}$  values were 28 and 20  $\mu\text{M}$  for 1 and 2 h incubation time, respectively. On further increasing the incubation time to 6 and 8 h, the  $\text{IC}_{50}$  value increased. Thus incubation for 4 h before photoirra-

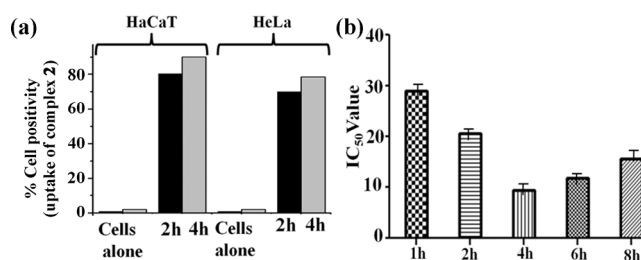


Figure 7. a) Uptake studies of complex **2** (16  $\mu\text{M}$ ) by FACS analysis in HaCaT and HeLa cells with the bar diagram showing % cell positivity at 2 and 4 h incubation times. b)  $\text{IC}_{50}$  values determined by MTT assay for complex **2** at different interval of incubation time prior to photoirradiation in HaCaT cells.

diation was chosen to obtain the  $\text{IC}_{50}$  values of the complexes **1** and **2** in HaCaT and HeLa cells.

**Cytotoxicity study:** The study was carried out for complexes **1** and **2** in HeLa and HaCaT cell lines in visible light of 400–700 nm and red light of 600–720 nm. The  $\text{IC}_{50}$  values of complex **2** were  $(9.4 \pm 0.2)$  and  $(13.5 \pm 0.1)$   $\mu\text{M}$  in HaCaT and HeLa cells, respectively, in visible light of 400–700 nm (Luzchem photoreactor, 10  $\text{J cm}^{-2}$ ) (Table 3, Figure 8a, and the Supporting Information, Figures S19 and S20). We also used a biomedical instrument for dermatological cancer or lesion treatment; a Waldmann PDT 1200L photoreactor of 600–720 nm wavelength range (150  $\text{J cm}^{-2}$ ). The photocytotoxici-

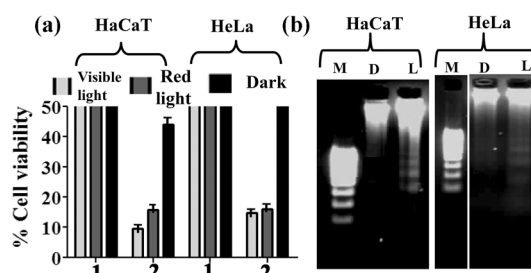


Figure 8. a) Bar diagram showing the photocytotoxicity of **1** and **2** in HaCaT and HeLa cells after 4 h incubation in the dark followed by 1 h exposure to visible light of 400–700 nm (10  $\text{J cm}^{-2}$ ) or red light of 600–720 nm (150  $\text{J cm}^{-2}$ ). b) DNA ladder of complex **2** (15  $\mu\text{M}$ ; D: dark, L: light, M: Marker, 100 bp).

Table 3.  $\text{IC}_{50}$  values of the oxidovanadium(IV) complexes, photofrin, and cisplatin in HaCaT and HeLa cells.

Compound	$\text{IC}_{50}$ [ $\mu\text{M}$ ]			
	HaCaT		HeLa	
	Light	Dark	Light	Dark
$[\text{VO}(\text{L}^1)(\text{phen})]\text{-Cl}$ ( <b>1</b> )	50	50	50	50
$[\text{VO}(\text{L}^2)(\text{L}^3)]\text{-Cl}$ ( <b>2</b> )	$9.4 \pm 0.2$ <sup>[a]</sup>	$44.1 \pm 0.3$	$13.5 \pm 0.1$ <sup>[a]</sup>	> 50
Photofrin <sup>[b]</sup>	–	–	$4.3 \pm 0.2$	> 41
Cisplatin <sup>[c]</sup>	–	$20.5 \pm 0.2$	–	–
Dppz-Gly-Gly-OMe	> 50	> 50	> 50	> 50
Hsal-an-ambmz	$7.7 \pm 0.3$	$12.1 \pm 0.2$	$14.1 \pm 0.4$	$24.9 \pm 0.1$

[a]  $\text{IC}_{50}$  value is  $(15.7 \pm 0.1)$  in HaCaT and  $(16.1 \pm 0.3)$   $\mu\text{M}$  in HeLa under red light of 600–720 nm wavelength (power: 150  $\text{J cm}^{-2}$ ). [b] Values taken from reference [32]. [c] Values taken from reference [33].

ty of complex **2** in both cells with this instrument was nearly three-fold higher in light than in dark with  $IC_{50}$  values of  $15.7 \mu\text{M}$  in HaCaT and  $16.1 \mu\text{M}$  in HeLa cells. The  $IC_{50}$  value was  $>50 \mu\text{M}$  for HeLa and  $44.1 \mu\text{M}$  in HaCaT cells in the dark. Complex **1** was nontoxic in both light and dark. A comparison of the  $IC_{50}$  values of **2** with other compounds is made in Table 3.<sup>[32,33]</sup> Complex **2** showed comparable PDT activity as reported for photofrin. Its dark toxicity is significantly less than that of cisplatin. The ligand Hsal-an-ambmz is photocytotoxic giving  $IC_{50}$  values of  $7.7$  and  $14.1 \mu\text{M}$  in light for HaCaT and HeLa cells, respectively. The ligand alone also showed significant dark cytotoxicity with  $IC_{50}$  values of  $12.1$  and  $24.9 \mu\text{M}$ . The formation of metal complexes thus reduces the dark toxicity of the anthracene ligand. Ligand  $L^3$ , that is, dppz-Gly-Gly-OMe, showed low cytotoxicity in dark and light giving  $IC_{50}$  value of  $>50 \mu\text{M}$ .

**DNA-laddering assay:** DNA laddering was performed for complex **2** ( $15 \mu\text{M}$ ) in HaCaT and HeLa cell lines to find out the mode of cell death, particularly the apoptotic mode of cell death. In apoptosis, the programmed cell death, the caspase-activated DNase (CAD) becomes activated and cleaves the DNA at internucleosomal linker site of approximately 180 base pairs (bp), which appears like a ladder when run in gel electrophoresis.<sup>[34]</sup> DNA fragmentation for complex **2** was observed in both HaCaT and HeLa cells only in the presence of light, whereas no such ladder appeared in dark (Figure 8b). This suggests that the complex is PDT-active only with light exposure causing the apoptotic cell death.

**Fluorescence microscopy:** Fluorescence microscopy experiments were conducted for complex **2** ( $15 \mu\text{M}$ ) having anthracene as a fluorescent tag in HaCaT and HeLa cell lines (Figure 9). Microscopy data suggest cytoplasmic localization

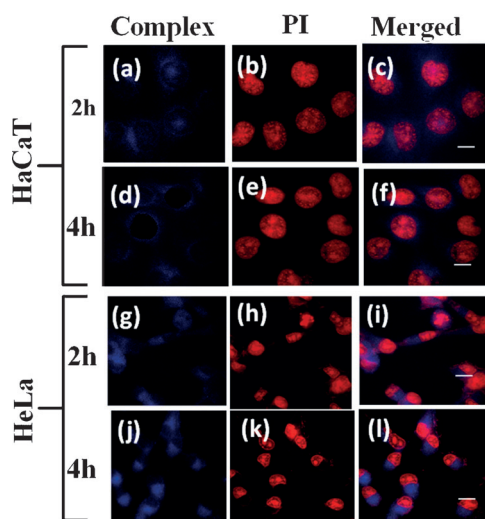


Figure 9. Fluorescence microscopic images of  $15 \mu\text{M}$  complex **2** in a)–f) HaCaT cells and g)–l) HeLa cells for 2 and 4 h. Panels a), d), g), and j) show fluorescence images of complex **2**. Panels b), e), h), and k) are for propidium iodide (PI) staining. Panels c), f), i), and l) are the merged images. Scale bar:  $10 \mu\text{m}$ .

of the complex in the cells. This observation is of importance considering that localization of the drug in cell nuclei is undesirable in PDT to avoid any potential damage to nuclear DNA, mutation, and carcinogenesis. The confocal studies were performed at two time points, that is, 2 and 4 h. From the confocal data it is apparent that complex **2** is capable of entering inside the cell within 2 h and is retained in the cells for 4 h. In contrast, the conjugated anthracenyl ligand (Hsal-an-ambmz) alone showed predominantly nuclear localization (Figure S21, the Supporting Information).

To visualise the PDT effect, complex **2** ( $15 \mu\text{M}$ ) was added to the HaCaT and HeLa cells and these were incubated for 4 h. One complex was exposed to visible light of 400–700 nm and another set was kept in dark (Figure 10). Fluorescence

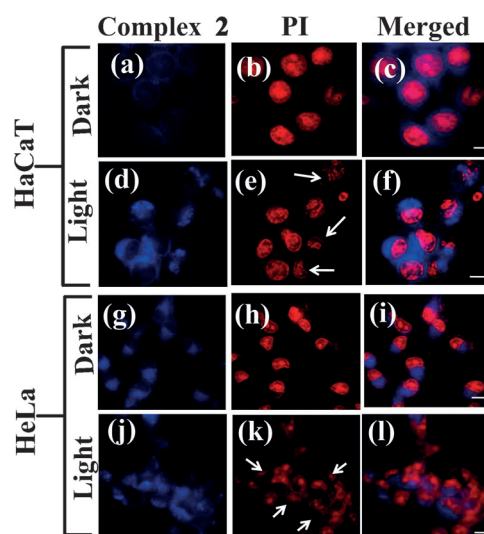


Figure 10. Fluorescence microscopic images of **2** ( $15 \mu\text{M}$ ) in a)–f) HaCaT cells and g)–l) HeLa cells. Panels a), d), g), and j) show fluorescence of **2**. Panels b), e), h), and k) are for PI staining. Panels c), f), i), and l) are the merged images. The PDT effect, visible only in light, is shown by arrow in panels e) and k). No PDT effect is visible in the dark (panels b) and h)). Scale bar:  $10 \mu\text{m}$ .

rescence images with one hour exposure to visible light exhibited irregular nuclear morphology on staining with propidium iodide (PI, red; Figure 10, panels (e, k)). Chromatin condensation of the nucleus was observed indicating apoptotic cell death as bright condensed nuclei were seen in photo-treated cells (Figure 10, panels (e, k)). In contrast, homogeneously PI-stained healthy nuclei were observed in dark after 4 h incubation for **2** (Figure 10, panels (b, h)). The results suggest cell death only in light with no apparent cell death in the dark.

**Targeting mitochondria:** With the knowledge of the complex accumulating in the cytoplasm, we were encouraged to probe further its specificity to any cellular organelle. For this specific purpose, we performed dual staining with mitotracker deep red, which stains mitochondria and complex **2** showing blue fluorescence. The experiment showed complex

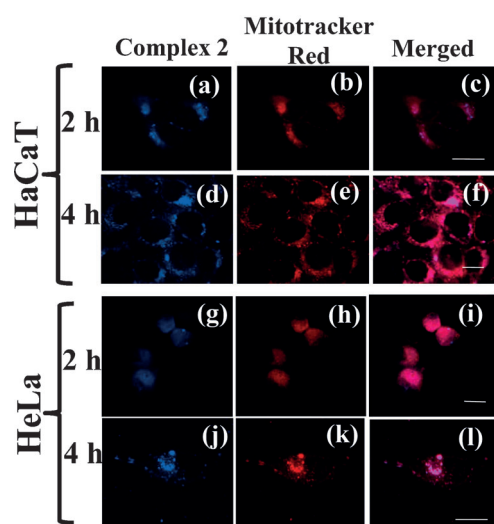


Figure 11. Fluorescence microscopic images of complex **2** (15  $\mu\text{M}$ ) in a)–f) HaCaT cells and g)–l) HeLa cells after 2 and 4 h showing the cellular uptake. Panels a), d), g), and j) show the fluorescence images of complex **2**. Panels b), e), h), and k) are fluorescence images of mitotracker red (50 nm for HaCaT and 20 nm for HeLa). Panels c), f), i), and l) are the merged fluorescence images of the mitotracker and the complex. Scale bar: 10  $\mu\text{m}$ .

**2** specifically localizing to the mitochondria in 4 h as evidenced from the merged images shown in Figure 11 (panels (f) and (l)). This new observation is of great significance because mitochondria plays key roles in mediating the intrinsic pathway of apoptosis. Thus, any alterations in the cancer cells leading to protection from apoptosis could be targeted. The results are of importance for cancer therapeutics since mitochondria plays an important role in cell apoptosis.<sup>[35–37]</sup> The FDA-approved drug photofrin is known to localize in the mitochondria for its drug action.<sup>[30]</sup>

**Mitochondrial membrane potential ( $\Delta\Psi_m$ ):** A decrease in the mitochondrial transmembrane potential ( $\Delta\Psi_m$ ) is one of the earliest intracellular events that occurs following the induction of apoptosis and it is an important parameter of mitochondrial functions and evaluates the apoptotic cell death. The damage of mitochondria leads to the depolarization of mitochondria with a drop in  $\Delta\Psi_m$ .<sup>[38]</sup> Rhodamine 123 (Rh123) dye was used as the mitochondrial fluorescence probe to study the mechanism of mitochondrial-regulated apoptosis for complex **2**. This dye is a fluorescent-green membrane-permeable mitochondrial dye that stains mitochondria in living cells. When used at higher concentrations ( $\approx 1 \mu\text{M}$ ), the dye will accumulate in the inner membrane of mitochondria and forms an aggregate resulting in the quenching of its green fluorescence. When mitochondrial membrane disruption occurs due to apoptosis, it leads to depolarization of the mitochondrial membrane potential. This results in the leakage of the dye from the mitochondria to the cytoplasm enhancing the green fluorescence intensity of the Rh123 dye, which was monitored by FACS in our study.

The experiments were conducted by using complex **2** (15  $\mu\text{M}$ ) in HeLa and HaCaT cells by FACS analysis

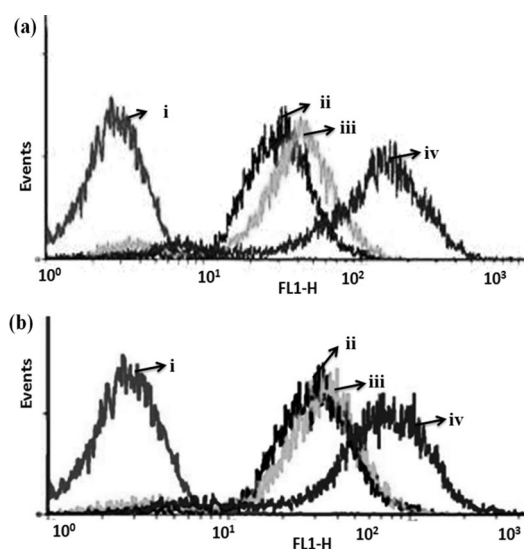


Figure 12. Flow cytometric analysis (FACS) of the mitochondrial membrane potential using rhodamine (Rh123) dye (1  $\mu\text{M}$ ) in a) HaCaT and b) HeLa cells: (i) corresponds to cells alone, (ii) corresponds to cells + Rh123 dye, (iii) corresponds to cells treated with complex **2** and Rh123 dye in dark, and (iv) corresponds to cells treated with complex **2** and Rh123 dye in visible light (400–700 nm).

(Figure 12 and the Supporting Information, Figure S22 and S23). The auto-fluorescence of cells is indicated in (i) of Figure 12, whereas (ii) is for the cells treated with Rh123 dye indicating quenching of Rhodamine 123 dye fluorescence. It was found to be similar to cells treated with **2** in dark suggesting no depolarization of mitochondria as shown by Figure 12 (iii). When cells treated with **2** were photoirradiated for 1 h, there was a shift in the peak towards right indicating an increase in the fluorescence intensity as shown by Figure 12 (iv). This proves that there is a depolarization of mitochondrial membrane potential taking place, which is a clear indication of apoptosis occurring on exposure to light. This implies that induction of apoptosis by **2** is associated with the mitochondrial (intrinsic) pathway. The mechanism is similar to photofrin, in which the PDT drug kills the cell by destabilizing the mitochondrial membrane.<sup>[39]</sup>

**ROS generation examined by the DCFDA assay:** The generation of reactive oxygen species (ROS) by complex **2** (15  $\mu\text{M}$ ) was examined by dichlorofluorescein diacetate (DCFDA) assay. DCFDA is a cell-permeable fluorogenic probe that undergoes oxidation to form 2',7'-dichlorofluorescein (DCF) showing an emission maximum at 528 nm (Figure 13). The quantitative measurement of ROS generation was performed by this assay using the FACS method. HeLa and HaCaT cells treated with complex **2** showed a shift in the fluorescence intensity upon photoirradiation compared with the cells treated with the complex but kept in the dark. This clearly proves that the increase in the intensity of fluorescence shown in Figure 13 (iv) is due to formation of the DCF dye, which is only possible from oxidation by ROS. To ascertain the role of ROS in mediating the

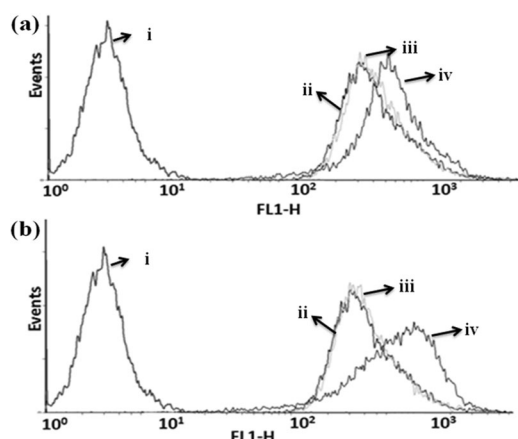


Figure 13. DCFDA/DCF assay performed for complex **2** (15  $\mu\text{M}$ ) for ROS generation in a) HaCaT and b) HeLa cells: (i) corresponds to cells alone, (ii) corresponds to cells + DCFDA dye, (iii) corresponds to cells treated with complex **2** and DCFDA dye in dark, and (iv) corresponds to cells treated with complex **2** and DCFDA dye in visible light (400–700 nm).

cytotoxicity, the cancer cells were treated with complex **2** and *N*-acetyl-L-cysteine (NAC) as the ROS quencher followed by photoirradiation and cytotoxicity was measured by the 3-(4,5-dimethylthiazol-2-yl)-2,5-diphenyltetrazolium bromide (MTT) assay.<sup>[40]</sup> It was observed that addition of NAC significantly reduced the activity of complex **2** giving an  $\text{IC}_{50}$  value, which is comparable to the dark cytotoxicity of the complex (Table 4 and Figure S24, the Supporting Information).

Table 4.  $\text{IC}_{50}$  values of complex **2** after 4 h incubation followed by exposure to visible light in absence and presence of NAC.

	$\text{IC}_{50}$ [ $\mu\text{M}$ ]		
	Light [400–700 nm]	Light + NAC [400–700 nm]	Dark
HaCaT	9.5( $\pm 0.2$ )	48.3( $\pm 0.5$ )	44.0( $\pm 0.1$ )
HeLa	14.8( $\pm 0.9$ )	> 50	> 50

**ROS generation in mitochondria:** To assess any light-mediated generation of ROS by complex **2** in the mitochondria, we performed a DCFDA assay followed by co-localization with the complex and the mitotracker (Figure 14). The fluorescence resulting from DCF formation was observed by using confocal microscopy. A yellow color was observed in the merged image with the mitotracker indicating the formation of ROS only in the mitochondria as shown in the panels (i) and (s) of Figure 14. The merged images of all three produce a pink/white color (Figure 14, panels (j) and (t)). The fluorescence intensity of DCF dye is negligible in dark as seen in Figure 14, panels (c) and (m). The intensity increases significantly upon photoirradiation. The data provide a direct evidence of ROS generation in the mitochondria of the cell by complex **2**, possibly by releasing mitochondrial components and triggering an apoptotic response.<sup>[20]</sup>

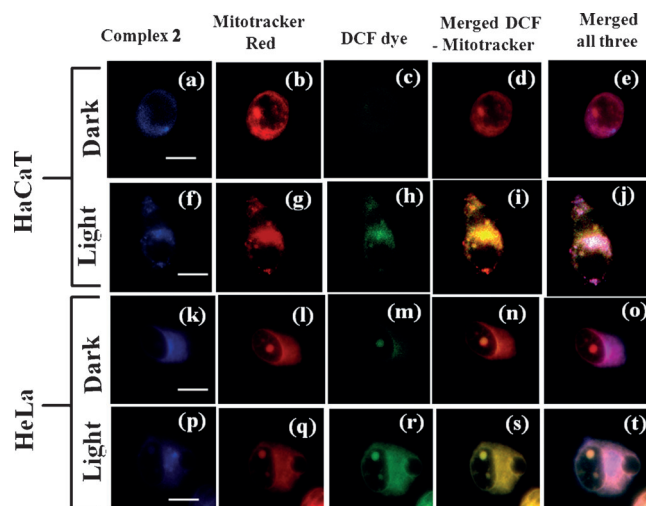


Figure 14. Fluorescence microscopic images of complex **2** (15  $\mu\text{M}$ ) in a)–j) HaCaT cells and k)–t) HeLa cells after 4 h incubation followed by exposure to visible light (400–700 nm) for 1.0 h. Panels a), f), k), p) show the fluorescence of complex **2**. Panels b), g), l), q) are the fluorescence images of the mitotracker (50 nM for HaCaT and 20 nM for HeLa). Panels c), h), m), r) show fluorescence of DCF dye. Panels d), i), n), and s) are merged images of the mitotracker and DCF. Panels e), j), o), and t) are merged images of all three. Scale bar: 10  $\mu\text{m}$ .

**Vanadium detection in mitochondria:** To further confirm the localization of complex **2** in the mitochondria, we detected the presence of vanadium in mitochondria by separating a sub-cellular fraction of HaCaT cells and isolating the mitochondria from treated (with complex **2**, 20  $\mu\text{M}$ ) and untreated cells. Isolated mitochondrial lysates were subjected to energy-dispersive X-ray spectroscopy (EDX) and the presence of vanadium  $\text{K}_{\alpha}$  and  $\text{K}_{\beta}$  peaks at 4.9 and 5.4 KeV were detected from the EDX spectrum only in the complex-treated mitochondrial lysates (Figure S25, the Supporting Information).<sup>[41]</sup>

## Conclusion

The oxidovanadium(IV) complex **2**, having an anthracenyl fluorophore and a dipeptide moiety, showed specific binding towards poly(dAdT)<sub>2</sub> base pairs and remarkable photocytotoxicity in near-IR light specifically targeting the mitochondria of the cancer cells. The localization of complex **2** in mitochondria is associated with the induction of apoptosis, which is caused by ROS generation on exposure to light (Figure S26, the Supporting Information). Complex **2**, showing significant PDT effect in near-IR light, is distinctly different from other known metal-based PDT agents and its activity compares well to that of the clinically approved PDT drug photofrin. The present results are expected to open up new avenues to develop mitochondria-targeting metal-based photochemotherapeutic agents with potential in vivo applications.

## Experimental Section

**Materials and methods:** All reagents and chemicals were purchased from commercial sources (s.d. Fine Chemicals, India; Sigma–Aldrich, U.S.A.) and used as such without further purifications. Solvents were purified by standard procedures.<sup>[42]</sup> (3-(4,5-Dimethylthiazol-2-yl)-2,5-diphenyltetrazolium bromide (MTT) and propidium iodide (PI), *N*-acetyl cysteine (NAC), and MitoTracker Deep Red FM (Cat. no.M22426) were purchased from Sigma (U.S.A.) and Invitrogen BioServices India.

The elemental analysis was done using a Thermo Finnigan Flash EA 1112 CHNS analyzer. The infrared and electronic spectra were recorded by using Bruker Alpha and PerkinElmer Spectrum 650 spectrophotometers, respectively. IR spectra signals are assigned as follows: br, broad; vs, very strong; s, strong; m, medium; w, weak. Emission spectral measurements were carried out with a PerkinElmer LS 55 spectrophotometer. Molar conductivity measurements were performed by using a Control Dynamics (India) conductivity meter. Cyclic voltammetric measurements were made at 25 °C on a EG&G PAR Model 253 VersaStat potentiostat/galvanostat with an electrochemical analysis software 270 using a three electrode set-up comprising a glassy carbon working electrode, a platinum wire auxiliary, and a saturated calomel reference (SCE) electrode. Tetrabutylammonium perchlorate (TBAP, 0.1 M) was used as a supporting electrolyte in DMF. The electrochemical data were uncorrected for junction potentials. Electrospray ionization mass spectral measurements were performed by using Esquire 3000 plus ESI (Bruker Daltonics) and Q-TOF Mass spectrometers. Confocal microscopy experiments were performed by using an Olympus IX81 confocal electron microscope (Leica, TCS SP5 DM6000). <sup>1</sup>H NMR spectral measurements were made using a Bruker 400 MHz NMR spectrometer. FACS Calibur (Becton Dickinson (BD) cell analyzer) at FL1 channel was used in the biological study. Magnetic susceptibility measurement of the complex at 300 K was performed with a powdered sample using MPMS SQUID VSM (Quantum Design, USA). Preparation of HL<sup>1</sup> and 9-bromomethyl anthracene was carried out by literature methods.<sup>[22,43]</sup>

**Synthesis of dppz-Gly-Gly-OMe:** *tert*-Butyloxycarbonyl (Boc)-protected 3,4-diaminobenzoic acid (1.0 g, 2.84 mmol) was treated with glycyl-glycine methyl ester hydrochloride (0.83 g, 4.5 mmol) to form amide coupling using *N,N*-dicyclohexylcarbodiimide (DCC; 0.86 g, 4.2 mmol) in 15 mL of dry DMF. On subsequent deprotection of Boc, the reaction mixture was treated with 1,10-phenanthroline dione (0.40 g, 1.9 mmol) to isolate dppz-Gly-Gly-OMe in ≈50% yield as an off-white solid (Scheme S1, the Supporting Information). <sup>1</sup>H NMR (400 MHz, [D<sub>6</sub>]DMSO): δ=9.24 (dd, *J*<sub>1</sub>=5.59 Hz, *J*<sub>2</sub>=5.72 Hz, 1H), 9.16–9.10 (m, 3H), 9.06 (d, *J*=4.2 Hz, 1H), 8.76 (dd, *J*<sub>1</sub>=5.73 Hz, *J*<sub>2</sub>=5.85 Hz, 1H), 8.46 (s, 1H), 8.18 (d, *J*=8.74, 1H), 8.05 (d, *J*=8.81 Hz, 1H), 7.86–7.83 (m, 1H), 7.80–7.77(m, 1H), 4.05 (d, *J*<sub>1</sub>=5.69 Hz, 2H), 4.01 (d, *J*<sub>1</sub>=5.84 Hz, 2H), 3.68 ppm (s, 3H); <sup>13</sup>C NMR (100 MHz, [D<sub>6</sub>]DMSO): δ=143.05, 141.97, 141.75, 141.42, 136.28, 133.74, 133.47, 131.01, 129.98, 129.85, 129.09, 127.97, 127.10, 125.16, 116.03, 55.01, 52.79, 43.41, 37.00 ppm; MS (ESI<sup>+</sup>, MeOH): *m/z* 455.74 [M+H]<sup>+</sup>.

**Synthesis of HL<sup>2</sup> (Hsal-an-ambmz):** Boc-protected glycine (1.71 g, 9.7 mmol) was treated with phenylene diamine (1.05 g, 9.7 mmol) to prepare the imidazole in ≈82% yield as an off-white solid. The anthracene fluorophore (1.64 g, 6.1 mmol) was attached to imidazole using NaH (60% suspension in mineral oil) (0.71 g, 30.0 mmol) in 10 mL dry THF. Boc was then deprotected to obtain the free amine, which was treated with salicylaldehyde (221 μL, 2.1 mmol) to isolate the Schiff base in ≈75% yield (0.68 g) (Scheme S1, the Supporting Information). <sup>1</sup>H NMR (400 MHz, CDCl<sub>3</sub>): δ=12.48 (s, 1H), 8.47 (s, 1H), 8.09 (d, *J*=8.6 Hz, 2H), 7.98 (d, *J*=6.2 Hz, 3H), 7.74 (d, *J*=8 Hz, 1H), 7.41 (dd, *J*<sub>1</sub>=4.2, *J*<sub>2</sub>=4 Hz, 4H), 7.28 (dd, *J*<sub>1</sub>=7.6, *J*<sub>2</sub>=7.4 Hz, 1H), 7.18 (dd, *J*<sub>1</sub>=7.4, *J*<sub>2</sub>=7.6 Hz, 1H), 7.02–6.99 (m, 2H), 6.92 (d, *J*=8.2, 1H), 6.84–6.76 (m, 2H), 6.30 (s, 2H), 4.84 ppm (s, 2H); <sup>13</sup>C NMR (100 MHz, CDCl<sub>3</sub>): δ=167.84, 161.09, 151.16, 142.92, 136.20, 133.19, 132.39, 131.71, 131.56, 130.31, 130.09, 127.94, 125.75, 124.56, 123.67, 123.43, 122.70, 120.46, 119.17, 118.97, 117.33, 111.09, 55.88, 42.38 ppm; MS (ESI<sup>+</sup>): *m/z*: 442.51 [M+H]<sup>+</sup> in MeOH.

**Synthesis of [VO(L<sup>1</sup>(phen))Cl (1) and [VO(L<sup>2</sup>(L<sup>3</sup>))Cl (2):** (HL<sup>1</sup>: Hsal-ambmz, HL<sup>2</sup>: Hsal-an-ambmz, L<sup>3</sup>: dppz-Gly-Gly-OMe): The complexes were prepared by following a general synthetic procedure in which vanadyl sulphate (0.18 g, 1.0 mmol) dissolved in MeOH (15 mL) was treated with a solution of BaCl<sub>2</sub> (0.24 g, 1.0 mmol). The mixture was stirred at an ambient temperature for 2 h. BaSO<sub>4</sub> thus precipitated was removed from the reaction mixture using Celite. The blue-coloured filtrate was initially reacted with the Schiff-base ligand HL<sup>1</sup> (0.25 g, 1.0 mmol) for complex **1** and ligand HL<sup>2</sup> (0.44 g, 1.0 mmol) for complex **2**. The solution colour changed to brown. The above solution was stirred for 45 min. The phenanthroline base (1.0 mmol) was added (0.29 g phen for **1** or 0.45 g dppz-Gly-Gly-OMe for **2**) and the solution was stirred further for 2 h to obtain a transparent yellow-brown solution. The resulting solution was filtered and the filtrate was allowed to evaporate. The filtrate on concentration gave a yellow solid on addition of diethyl ether. The solid was isolated, washed with cold methanol, crystallized from methanol and finally dried in vacuum over P<sub>4</sub>O<sub>10</sub>.

**[VO(L<sup>1</sup>(phen))Cl (1):** Yield: 0.39 g (≈75%); Λ<sub>M</sub>=70 Sm<sup>2</sup>M<sup>-1</sup> in DMF at 25 °C; IR (KBr):  $\tilde{\nu}$ =3364 (br), 3055 (w), 1614 (vs, C=N), 1539 (m), 1469 (w), 1414 (m), 1295 (m), 1199 (w), 1150 (w), 1047 (w), 960 (s, V=O), 908 (w), 850 (m), 723 (s), 616 (m), 431 (m), 574 cm<sup>-1</sup> (w); UV/Vis (50% aq DMF): λ<sub>max</sub> (ε): 693 (40), 400 (2460), 291 (15660), 272 nm (33310 dm<sup>3</sup>M<sup>-1</sup>cm<sup>-1</sup>); μ<sub>eff</sub>=1.64 μ<sub>B</sub>; ESI-MS in MeOH: *m/z* 497.33 [M]<sup>+</sup>; elemental analysis calcd (%) for C<sub>27</sub>H<sub>20</sub>ClN<sub>5</sub>O<sub>2</sub>V: C 60.86, H 3.78, N 13.14; found: C 60.64, H 3.63, N 13.06.

**[VO(L<sup>2</sup>(dppz-Gly-Gly-OMe))Cl (2):** Yield: 0.64 g (≈65%); Λ<sub>M</sub>=73 Sm<sup>2</sup>M<sup>-1</sup> in DMF at 25 °C; IR (KBr):  $\tilde{\nu}$ =3277 (br), 3047 (w), 1739 (w), 1551 (m), 1614 (vs) (C=N), 1537 (s), 1492 (m), 1443 (m), 1405 (s), 1360 (w), 1290 (m), 1029 (w), 964 (s) (V=O), 904 (w), 820 (w), 734 (vs), 619 (w), 562 (w), 420 cm<sup>-1</sup> (m); UV/Vis (50% aq DMF): λ<sub>max</sub> (ε): 672 (90), 386 (17770), 370 (19360), 352 (14740), 291 sh (40490), 276 (66470), 256 nm (76390 dm<sup>3</sup>M<sup>-1</sup>cm<sup>-1</sup>); μ<sub>eff</sub>=1.63 μ<sub>B</sub>; ESI-MS in MeOH: *m/z* 961.53 [M]<sup>+</sup>; elemental analysis calcd (%) for C<sub>34</sub>H<sub>40</sub>ClN<sub>9</sub>O<sub>6</sub>V: C 65.03, H 4.04, N 12.64; found: C 64.89, H 4.17, N 12.60.

**Solubility and stability:** The complexes were soluble in MeOH, EtOH, DMF and DMSO, moderately soluble in water; less soluble in MeCN, CH<sub>2</sub>Cl<sub>2</sub> and insoluble in hydrocarbons. They were stable in both solid and solution phases.

Time-dependent cathodic scan for **2** showed no apparent change in the cathodic peak current (*i*<sub>pc</sub>) after 8 h indicating stability of the complex (Figure S12e, the Supporting Information). The stability of **2** was also studied by time-dependent UV/Visible spectroscopy in 1% DMSO in DPBS buffer to maintain the cellular condition. The titration data showed no apparent change in the spectral features even after 24 h. We also checked the stability of complex **2** after and before 1 h photoirradiation and the complexes were found to be stable (Figure S27, the Supporting Information).

**X-ray crystallographic procedures:** The crystal structure of complex **1** as its perchlorate salt (**1a**-EtOH) was obtained by using the single-crystal X-ray diffraction method. Crystals were obtained on slow evaporation of the ethanol/acetone solution of the complex in the presence of perchlorate anion. Crystal mounting was done on glass fiber with epoxy cement. All geometric and intensity data were collected at 22 °C using an automated Bruker SMART APEX CCD diffractometer equipped with a fine focus 1.75 kW sealed tube MoK<sub>α</sub> X-ray source (λ=0.71073 Å) with increasing ω (width of 0.3° per frame) at a scan speed of 5 s per frame. Intensity data, collected using ω–2θ scan mode, were corrected for Lorentz-polarization effects and for absorption.<sup>[44]</sup> The structure was solved by the combination of Patterson and Fourier techniques and refined by full-matrix least-squares method by using the SHELX system of programs.<sup>[24]</sup> All hydrogen atoms belonging to the complex were in their calculated positions and refined using a riding model. All non-hydrogen atoms were refined anisotropically. CCDC-928547 (**1a**-EtOH), contains the supplementary crystallographic data for this paper. These data can be obtained free of charge from The Cambridge Crystallographic Data Centre via www.ccdc.cam.ac.uk/data\_request/cif. Selected crystallographic parameters are given in Table 5.

Table 5. Selected crystallographic data for [VO(L<sup>1</sup>)(phen)][ClO<sub>4</sub>] $\cdot$ EtOH (**1a** $\cdot$ EtOH).

Formula	C <sub>29</sub> H <sub>26</sub> ClN <sub>5</sub> O <sub>7</sub> V
Crystal size [mm <sup>3</sup> ]	0.40 $\times$ 0.33 $\times$ 0.19
$F_w$ [g M <sup>-1</sup> ]	642.94
Crystal system	Triclinic
Space group (No.)	$P\bar{1}$ (2)
$a$ [Å]	10.846(5)
$b$ [Å]	11.443(5)
$c$ [Å]	12.083(5)
$\alpha$ [°]	95.046(5)
$\beta$ [°]	101.405(5)
$\gamma$ [°]	96.276(5)
$V$ [Å <sup>3</sup> ]	1451.9(11)
$Z$	2
$T$ [K]	293(2)
Density (calcd) [g cm <sup>-3</sup> ]	1.471
$\lambda$ [Å] (MoK $\alpha$ )	0.71073
$\mu$ [mm <sup>-1</sup> ]	0.489
Data/restraints/parameters	6280/0/388
Goodness-of-fit on $F^2$	1.024
$R$ ( $F_o$ ) <sup>[a]</sup> [ $I > 2\sigma(I)$ ]	0.0940
$wR$ ( $F_o$ ) <sup>[b]</sup> [ $I > 2\sigma(I)$ ]	0.2553
$R$ [all data] ( $wR$ [all data])	0.1806 (0.3142)
Largest diff. peak and hole [e Å <sup>-3</sup> ]	1.014, -0.810

[a]  $R = \sum |F_o| - |F_c| / \sum |F_o|$ , [b]  $wR = [\sum (w(F_o^2 - F_c^2)^2) / \sum (w(F_o^2)^2)]^{1/2}$ ;  $w = [\sigma^2(F_o^2) + (AP)^2 + BP]^{-1}$ , in which  $P = (F_o^2 + 2F_c^2)/3$ ;  $A$  and  $B$  values are 0.1777 and 0.0000, respectively.

**DNA-binding and cleavage experiments:** The DNA-binding experiments were carried out by using calf thymus (ct)-DNA by following reported methods.<sup>[45]</sup> DNA-melting experiments were performed by monitoring the absorption intensity of ct-DNA at 260 nm at various temperatures, both in the absence and presence of the oxidovanadium(IV) complexes. The viscosity measurements were done by using a Schott Gerate AVS 310 automated viscometer attached with constant temperature bath at 37°C. The concentration of ct-DNA stock solution was 140  $\mu$ M (NP) in nucleotide pair in 5 mM Tris-HCl buffer. UV/Vis absorption titration experiments were carried out by using ct-DNA, poly(dAdT)<sub>2</sub>, and poly(dGdC)<sub>2</sub> (ca. 200  $\mu$ M) in 5 mM Tris-HCl buffer medium with a fixed metal-complex concentration of 25  $\mu$ M. The DNA cleavage of supercoiled pUC19 DNA (30  $\mu$ M, 0.2  $\mu$ g, 2686 base pairs) was studied by agarose gel electrophoresis using complexes **1** and **2** (50  $\mu$ M) in Tris-HCl buffer (50 mM) of pH 7.2 containing NaCl (50 mM). Photoinduced DNA-cleavage experiments in visible light were done using a diode laser of 705 nm wavelength (LQC705-38E of Newport Corporation, power 40 mW). After light exposure, each sample was incubated for 30 min at 37°C and analyzed for the photocleaved products using gel electrophoresis. The mechanistic studies were carried out using different singlet-oxygen quenchers and hydroxyl-radical scavengers to detect formation of any reactive oxygen species (ROS).

**Cell cytotoxicity assay:** The photocytotoxicity of **1** and **2** was studied by using the MTT assay with quantification of formazan formed by cleavage of the tetrazolium rings of MTT in DMSO by spectral measurements.<sup>[46]</sup> Various concentrations of the complex dissolved in 1% DMSO were added to the cells and incubation was continued for 4 h in dark followed by photoirradiation with visible light of 400–700 nm (10 J cm<sup>-2</sup>) and red light of 600–720 nm (150 J cm<sup>-2</sup>) by using a Luzchem Photoreactor (Model LZC-1, Ontario, Canada) fitted with Sylvania make 8 fluorescent white tubes and Waldmann PDT 1200L, respectively. After the incubation period of 20 h, MTT (5 mg mL<sup>-1</sup>) was added to each well and incubated for an additional 3 h. The IC<sub>50</sub> values were obtained by nonlinear regression analysis (GraphPad Prism).

**DNA fragmentation analysis by agarose gel electrophoresis:** Briefly, HaCaT and HeLa cells (0.3  $\times$  10<sup>6</sup>) were taken in each 60 mm dish.<sup>[47]</sup> They were grown for 24 h and later treated with the complex for 4 h in the dark. Samples were exposed to light in one of the dish for 1 h and again

the cells were allowed to grow for 12 h along with its dark control. After 12 h, cells were trypsinized, washed with DPBS and re-suspended in 0.4 mL of lysis buffer (10 mM Tris-HCl; pH, 8.0, 20 mM EDTA, 0.2% triton-X 100) with an incubation time of 20 min on ice. Lysed cells were centrifuged for 20 min at 13000 rpm and their supernatant was collected. Phenol chloroform was performed to remove the protein present. The supernatant was precipitated with 1:10 volume of 3 M sodium acetate (pH 5.8) and 2 volumes of ethanol at -20°C overnight. The DNA pellet was washed with 70% ethanol and re-suspended in TE containing RNase (1X Tris-EDTA with 100  $\mu$ g mL<sup>-1</sup> RNase) followed by an incubation for 2 h at 37°C. DNA samples were loaded on 1.5% agarose gel, which was run at 70 V for approximately 2 h before being photographed under UV light.

**Fluorescence microscopy experiments:** Localization of the fluorescent complex **2** into the HeLa and HaCaT cells was studied by using an Olympus 1X81 confocal electron microscope.<sup>[48]</sup> HeLa or HaCaT cells were grown on glass cover slips in each 12-well plates at a seeding density of 5.0  $\times$  10<sup>4</sup> cells in the culture medium (1.5 mL) for 24 h. The cells were subsequently treated with the complex for 2–4 h in dark. Cells were then fixed and permeabilized with chilled methanol for 5 min at -20°C. Methanol was removed and the cells were stored at -20°C for 6 h. The cells were then washed with 1  $\times$  PBS and incubated with propidium iodide (PI, 10 mg mL<sup>-1</sup>, diluted to 1:4) to stain the nucleus for 2 min before being visualized under a confocal microscope. To view the PDT effect, we performed the experiment by exposing one of the dishes to visible light for 45 min. The cell-permeable MitoTracker deep red, having a mildly thiol-reactive chloromethyl moiety, was used for labeling mitochondria. MitoTracker Deep Red FM (Cat. no.M22426, 20 nm) was used for confocal microscopy.<sup>[20a]</sup> A confocal experiment was performed for the detection of ROS generation in mitochondria by using a dual-staining procedure with DCFDA dye in a similar manner as the mitotracker experiment, but after the incubation period the cells were washed with PBS again, then incubated with DCFDA (1  $\mu$ M) for 20 min in PBS at 25°C. Finally, cells were washed with PBS and cover slips were mounted on slides and were visualised under a confocal microscope.

**Flow cytometry for mitochondrial membrane potential:** To assess the mitochondrial membrane potential, rhodamine123 (Rh123), a fluorescent-green membrane-permeable mitochondrial dye that stains mitochondria in living cells in a membrane potential-dependent fashion, was used. In flow cytometric analysis for the detection of mitochondrial membrane potential, HeLa or HaCaT cells (5.0  $\times$  10<sup>4</sup>) were plated in the culture medium (1.5 mL) for 24 h. These cells were incubated with the complex **2** (15  $\mu$ M) for 4 h followed by photoirradiation (400–700 nm) for 30 min in PBS. The cells were harvested by trypsinization and a single cell suspension of 1  $\times$  10<sup>6</sup> cells mL<sup>-1</sup> was made in PBS. The cells were then treated with a final concentration of Rh123 solution (1  $\mu$ M) in PBS for 15–20 min at room temperature. The distribution of Rh123 stained cells was determined by flow cytometry in the FL-1 channel.

**ROS generation from DCFDA:** The dihydro-analogue of the fluorescent probe, 2',7'-dichlorofluorescein diacetate (DCFDA) was used to detect the generation of cellular reactive oxygen species (ROS). Cell-permeable DCFDA when oxidized by cellular ROS generates a fluorescent compound DCF having an emission maxima at 528 nm.<sup>[49]</sup> The percentage of the cell population generating ROS could be determined either by flow cytometry analysis or by fluorescence microscopy. In flow cytometric analysis to detect ROS generation, HeLa cells were incubated with the complex **2** (15  $\mu$ M) for 4 h followed by photoirradiation (400–700 nm) for 30 min in serum free conditions. The cells were harvested by trypsinization and a single cell suspension of 1  $\times$  10<sup>6</sup> cells mL<sup>-1</sup> was made. The cells were then treated with DCFDA solution (1.0  $\mu$ M) in DMSO in dark for 15–20 min at room temperature. The distribution of DCFDA-stained HeLa cells was determined by flow cytometry in the FL-1 channel.

**DFT study:** The geometry of complex **2** was optimized by density functional theory (DFT) by using Gaussian 03.<sup>[50]</sup> For optimization, the B3LYP functional was used employing two types of basis sets, that is, 6-31G for lighter elements (C, N, H, O) and LanL2DZ for the heavier element (vanadium).<sup>[51]</sup>

**Lifetime measurement of the excited state:** The lifetime of the excited state for complex **2** was measured in DMSO solvent by Horiba Jobin Yvon Fluorocube-01-NL Fluorescence Lifetime System equipment. The complex was excited at 374 nm and emission was recorded at 419 nm.

**Isolation of mitochondria and EDX analysis:** Isolation of mitochondria from cells was performed following a published protocol.<sup>[52]</sup> The mitochondrial lysates collected from treated and control cells was subjected to energy-dispersive X-ray spectroscopy (EDX/EDS). Purity of mitochondrial and nuclear lysates was determined by semi-quantitative PCR by using human ND1 (NADH dehydrogenase subunit 1) gene specific primer pairs (F-5' CTAGCCATCATCTACTATCAAC 3' and R-5' AG-GAGTAATCAGAGGTGTTTC 3'; Amplicon 92 bp).

## Acknowledgements

We thank the Department of Science and Technology (DST), Government of India, and the Council of Scientific and Industrial Research (CSIR), New Delhi, for financial support (SR/S5/MBD-02/2007; CSIR/01(2559)/12/EMR-II/2012). We thank the Alexander von Humboldt (AvH) Foundation, Germany, for an electrochemical system. A.R.C. thanks DST for J. C. Bose Fellowship. I.K. thanks CSIR for a research fellowship. We thank Bappaditya Gole for the DFT data.

- [1] M. Ethirajan, Y. Chen, P. Joshi, R. K. Pandey, *Chem. Rev.* **2011**, *40*, 340–362.
- [2] J. P. Celli, B. Q. Spring, I. Rizvi, C. L. Evans, K. S. Samkoe, S. Verma, B. W. Pogue, T. Hasan, *Chem. Rev.* **2010**, *110*, 2795–2838.
- [3] A. Kamkaew, S. H. Lim, H. B. Lee, L. V. Kiew, L. Y. Chung, K. Burgess, *Chem. Rev.* **2013**, *42*, 77–88.
- [4] R. Bonnett, *Chemical Aspects of Photodynamic Therapy*, Gordon & Breach: London, **2000**.
- [5] P. Couleaud, V. Morosini, C. Frochot, S. Richeter, L. Raehm, J.-O. Durand, *Nanoscale* **2010**, *2*, 1083–1095.
- [6] P. Agostinis, K. Berg, K. A. Cengel, T. H. Foster, A. W. Girotti, S. O. Gollnick, S. M. Hahn, M. R. Hamblin, A. Juzeniene, D. Kessel, M. Korbelik, J. Moan, P. Mroz, D. Nowis, J. Piette, B. C. Wilson, J. Golab, *CA Cancer J. Clin.* **2011**, *61*, 250–281.
- [7] S. B. Brown, E. A. Brown, I. Walker, *Lancet Oncol.* **2004**, *5*, 497–508.
- [8] A. B. Ormond, H. S. Freeman, *Materials* **2013**, *6*, 817–840.
- [9] K. Szacilowski, W. Macyk, A. Drezewiecka-Matuszek, M. Brindell, G. Stochel, *Chem. Rev.* **2005**, *105*, 2647–2694.
- [10] a) C. J. Burrows, J. G. Muller, *Chem. Rev.* **1998**, *98*, 1109–1152; b) Y. Sun, L. E. Joyce, N. M. Dickson, C. Turro, *Chem. Commun.* **2010**, *46*, 6759–6761.
- [11] a) N. J. Farrer, J. A. Woods, L. Salassa, Y. Zhao, K. S. Robinson, G. Clarkson, F. S. Mackay, P. J. Sadler, *Angew. Chem.* **2010**, *122*, 9089–9092; *Angew. Chem. Int. Ed.* **2010**, *49*, 8905–8908; b) F. S. Mackay, J. A. Woods, P. Heringová, J. Kašpárková, A. M. Pizarro, S. A. Moggach, S. Parsons, V. Brabec, P. J. Sadler, *Proc. Natl. Acad. Sci. USA* **2007**, *104*, 20743–20748.
- [12] a) N. L. Fry, P. K. Mascharak, *Acc. Chem. Res.* **2011**, *44*, 289–298; b) A. A. Eroy-Reveles, Y. Leung, C. M. Beavers, M. M. Olmstead, P. K. Mascharak, *J. Am. Chem. Soc.* **2008**, *130*, 6650–6650; c) P. C. Ford, *J. Am. Chem. Soc.* **2009**, *131*, 15963–15964.
- [13] a) P. K. Sasmal, S. Saha, R. Majumdar, R. R. Dighe, A. R. Chakravarty, *Chem. Commun.* **2009**, 1703–1705; b) U. Basu, I. Khan, A. Hussain, P. Kondaiah, A. R. Chakravarty, *Angew. Chem.* **2012**, *124*, 2712–2715; *Angew. Chem. Int. Ed.* **2012**, *51*, 2658–2661.
- [14] S. Banerjee, P. Prasad, A. Hussain, I. Khan, P. Kondaiah, A. R. Chakravarty, *Chem. Commun.* **2012**, *48*, 7702–7704.
- [15] a) S. Fulda, L. Galluzzi, G. Kroemer, *Nat. Rev. Drug Discovery* **2010**, *9*, 447–467; b) J. S. Armstrong, *Br. J. Pharmacol.* **2006**, *147*, 239–248.
- [16] a) S. Marrachea, S. Dhar, *Proc. Natl. Acad. Sci. USA* **2012**, *109*, 16288–16293; b) S. Marrachea, S. Tundup, D. A. Harn, S. Dhar, *ACS Nano* **2013**, *7*, 7392–7402.
- [17] C. E. Wenner, *J. Cell. Physiol.* **2012**, *227*, 450–456.
- [18] J. Saczko, M. Mazurkiewicz, A. Chwilkowska, J. Kulbacka, G. Kramer, M. Ługowski, M. Śnietura, T. Banas, *Folia Biol.* **2007**, *53*, 7–12.
- [19] P. Mroz, A. Yaroslavsky, G. B. Kharkwal, M. R. Hamblin, *Cancers* **2011**, *3*, 2516–2539.
- [20] a) M. Lam, N. L. Oleinick, A.-L. Nieminen, *J. Biol. Chem.* **2001**, *276*, 47379–47386; b) R. Hilf, *J. Bioenerg. Biomembr.* **2007**, *39*, 85–89.
- [21] K. Nakamoto, *Infrared and Raman Spectra of Inorganic and Coordination Compounds*, Wiley, Hoboken, **1997**.
- [22] M. R. Maurya, A. Kumar, M. Ebel, D. Rehder, *Inorg. Chem.* **2006**, *45*, 5924–5937.
- [23] D. K. Balta, N. Arsu, Y. Yagci, S. Jockusch, N. J. Turro, *Macromolecules* **2007**, *40*, 4138–4141.
- [24] a) G. M. Sheldrick, SHELX-97, Programs for Crystal Structure Solution and Refinement; University of Göttingen, Göttingen, Germany, 1997; b) C. K. Johnson, ORTEP, Report ORNL-5138; Oak Ridge National Laboratory: Oak Ridge, TN, 1976.
- [25] P. Prasad, P. K. Sasmal, I. Khan, P. Kondaiah, A. R. Chakravarty, *Inorg. Chim. Acta* **2011**, *372*, 79–87.
- [26] G. L. Eichhorn, Y. A. Shin, *J. Am. Chem. Soc.* **1968**, *90*, 7323–7328.
- [27] J. M. Veal, R. L. Rill, *Biochemistry* **1991**, *30*, 1132–1140.
- [28] J. D. McGhee, P. H. von Hippel, *J. Mol. Biol.* **1974**, *86*, 469–489.
- [29] M. T. Carter, M. Rodriguez, A. J. Bard, *J. Am. Chem. Soc.* **1989**, *111*, 8901–8911.
- [30] R. J. Singh, H. Karoui, M. R. Gunther, J. S. Beckman, R. P. Manson, B. Kalyanaraman, *Proc. Natl. Acad. Sci. USA* **1998**, *95*, 6675–6680.
- [31] R. Weissleder, K. Kelly, E. Y. Sun, T. Shtatland, L. Josephson, *Nat. Biotechnol.* **2005**, *23*, 1418–1423.
- [32] E. Delaey, F. Van Laar, D. De Vos, A. Kamuhabwa, P. Jacobs, P. De Witte, *J. Photochem. Photobiol. B* **2000**, *55*, 27–36.
- [33] E. L. M. Wong, G. S. Fang, C. M. Chi, N. Zhu, *Chem. Commun.* **2005**, 4578–4580.
- [34] D. M. Conrad, S. J. Furlong, C. D. Doucette, K. A. West, D. W. Hoskin, *Apoptosis* **2010**, *15*, 597–607.
- [35] C. Stroh, K. Schulze-Osthoff, *Cell Death Differ.* **1998**, *5*, 997–1000.
- [36] S. W. G. Tait, D. R. Green, *Nat. Rev. Mol. Cell Biol.* **2010**, *11*, 621–632.
- [37] B. Favaloro, N. Allocati, V. Graziano, C. D. Iliio, V. D. Laurenzi, *Aging* **2012**, *4*, 330–349.
- [38] S. W. Perry, J. P. Norman, J. Barbieri, E. B. Brown, H. A. Gelbard, *Biotechniques* **2011**, *50*, 98–115.
- [39] a) S. Wu, D. Xing, *J. X-Ray Sci. Technol.* **2013**, *20*, 363–372; b) I. Kinzler, E. Haserth, C. Hauser, A. Rück, *Photochem. Photobiol. Sci.* **2007**, *6*, 1332–1340.
- [40] W. Y. Choi, B. T. Choi, W. H. Lee, Y. H. Choi, *Biomed. Pharmacother.* **2008**, *62*, 637–644.
- [41] T. Kuwabara, H. Kurishita, M. Hasegawa, *J. Nucl. Mater.* **2000**, *283–287*, 611–615.
- [42] D. D. Perrin, W. L. F. Armarego, D. R. Perrin, *Purification of Laboratory Chemicals*; Pergamon Press, Oxford, **1980**.
- [43] J. R. Shah, P. D. Mosier, B. L. Roth, G. E. Kellogg, R. B. Westkaemper, *Bioorg. Med. Chem.* **2009**, *17*, 6496–6504.
- [44] N. Walker, D. Stuart, *Acta Crystallogr. Sect. A* **1983**, *39*, 158–166.
- [45] P. Prasad, P. K. Sasmal, R. Majumdar, R. R. Dighe, A. R. Chakravarty, *Inorg. Chim. Acta* **2010**, *363*, 2743–2751.
- [46] T. Mosmann, *J. Immunol. Methods* **1983**, *65*, 55–63.
- [47] P. T. Daniel, I. Sturm, S. Ritschel, K. Friedrich, B. Dörken, P. Bendzko and T. Hillebrand, *Anal. Biochem.* **1999**, *266*, 110–115.
- [48] a) P. Prasad, I. Khan, P. K. Sasmal, D. Koley, P. Kondaiah, A. R. Chakravarty, *Dalton Trans.* **2013**, *42*, 4436–4449; b) P. Prasad, I. Khan, P. K. Sasmal, D. Koley, P. Kondaiah, A. R. Chakravarty, *Chem. Commun.* **2011**, *47*, 3954–3956.
- [49] T. Takahashi, Y. Ogura, H. Taguchi, M. Hashizoe, Y. Honda, *Invest. Ophthalmol. Vis. Sci.* **1997**, *38*, 2721–2728.

- [50] Gaussian 03, Revision B.4, M. J. Frisch, G. W. Trucks, H. B. Schlegel, G. E. Scuseria, M. A. Robb, J. R. Cheeseman, J. A. Montgomery, T. Vreven, K. N. Kudin, J. C. Burant, J. M. Millam, S. S. Iyengar, J. Tomasi, V. Barone, B. Mennucci, M. Cossi, G. Scalmani, N. Rega, G. A. Petersson, H. Nakatsuji, M. Hada, M. Ehara, K. Toyota, R. Fukuda, J. Hasegawa, H. Ishida, T. Nakajima, Y. Honda, O. Kitao, H. Nakai, M. Klene, X. Li, J. E. Knox, H. P. Hratchian, J. B. Cross, C. Adamo, J. Jaramillo, R. Gomperts, R. E. Stratmann, O. Yazyev, A. J. Austin, R. Cammi, C. Pomelli, J. Ochterski, P. Y. Ayala, K. Morokuma, G. A. Voth, P. Salvador, J. J. Dannenberg, V. G. Zakrzewski, S. Dapprich, A. D. Daniels, M. C. Strain, O. Farkas, D. K. Malick, A. D. Rabuck, K. Raghavachari, J. B. Foresman, J. V. Ortiz, Q. Cui, A. G. Baboul, S. Clifford, J. Cioslowski, B. B. Stefanov, G. Liu, A. Liashenko, P. Piskorz, I. Komaromi, R. L. Martin, D. J. Fox, T. Keith, M. A. Al-Laham, C. Y. Peng, A. Nanayakkara, M. Challacombe, P. M. W. Gill, B. Johnson, W. Chen, M. W. Wong, C. Gonzalez, J. A. Pople, Gaussian Inc.: Pittsburgh, PA, **2003**.
- [51] A. D. Becke, *J. Chem. Phys.* **1993**, *98*, 5648–5652.
- [52] J. M. Graham, *Isolation of mitochondria from tissues and cells by differential centrifugation. Curr Protoc Cell Biol* **2001**, Chap. 3, Unit 33.

Received: September 4, 2013  
Published online: November 13, 2013